Catalysis Today 161 (2011) 46–52

Contents lists available at ScienceDirect

Catalysis Today

journal homepage: www.elsevier.com/locate/cattod

Nitrogen-doped TiO_2/AC bi-functional composite prepared by two-stage calcination for enhanced synergistic removal of hydrophobic pollutant using solar irradiation

Pow-Seng Yap [a], Teik-Thye Lim [a,*], Madhavi Srinivasan [b]

[a] School of Civil and Environmental Engineering, Nanyang Technological University, 50 Nanyang Avenue, Singapore 639798, Singapore
[b] School of Materials Science and Engineering, Nanyang Technological University, 50 Nanyang Avenue, Singapore 639798, Singapore

ARTICLE INFO

Article history:
Available online 3 November 2010

Keywords:
Titania
Nitrogen doping
Activated carbon
Photocatalytic degradation
Hydrophobic pollutants
Solar irradiation

ABSTRACT

Sol–gel method with the incorporation of two-stage calcination protocol was developed to synthesize a bi-functional composite, viz. nitrogen-doped titanium dioxide supported on activated carbon (N-TiO_2/AC). Various types of N-TiO_2/AC composites produced using different calcination conditions were characterized using XRD, porosimetry, XPS, SEM and TEM. All the N-TiO_2/AC composites exhibited good adsorption of a hydrophobic pollutant (bisphenol-A (BPA) as model pollutant) in water. The effects of calcination conditions, light wavelength and composite dosage on photocatalytic degradation (PCD) performance were investigated. N-TiO_2/AC (400M-700T) composite produced from two-stage calcination (400 °C in air with subsequent 700 °C in NH_3/N_2 atmosphere) was comprised of anatase–rutile phase and this composite exhibited significant PCD efficiency for removing BPA under simulated solar irradiation, with initial pseudo first-order rate constant of ca. 0.67 h^{-1}. In addition, the N-TiO_2/AC composite exhibited satisfactory BPA removal performance over several series of reuse. Photostability of the N-TiO_2/AC composite was also examined to address its durability under prolonged exposure of UV irradiation. The amount of carbon being leached in water was found to be less than 0.1% after 6 h of UV irradiation.

1. Introduction

Over the past decades, semiconductor photocatalysis has attracted intense scientific interest due to its huge potential for the destruction of various recalcitrant pollutants. Among the various types of semiconductors, titanium dioxide (TiO_2) has emerged as the leading candidate for continuous investigation because it is commercially available, of low toxicity, chemically and biologically stable, inexpensive, and it exhibits remarkable photocatalytic activity upon excitation by UV irradiation [1].

However, practical application of bare TiO_2 powders are faced with two major limitations. The first challenge is poor separation of TiO_2 nanoparticles from the treated water. To overcome this problem, many researchers have developed TiO_2 supported systems, using either organic [2,3] and inorganic [4,5] materials. Since semiconductor photocatalysis is a surface-mediated reaction, TiO_2 supports which can reduce mass transfer limitation would be desirable. In consideration of the various organic pollutants omnipresent in contaminated waters, carbonaceous supports for TiO_2 are appealing since they have high affinity for organic substances. Among the types of carbonaceous supports, activated carbon (AC) is the most promising candidate because it: (a) possesses excellent affinity for a myriad of organics, especially the hydrophobic and non-polar contaminants, (b) is readily available at various particle sizes, (c) suitable for water treatment applications, and (d) has been reported to enhance photonic efficiency for the supported TiO_2 by increasing the time-scale of charge carriers separation [6]. Furthermore, despite AC being a black color support, recent research on TiO_2/AC revealed encouraging experimental results whereby photocatalytic activity exhibited by TiO_2/AC with appropriate dosages greatly surpassed that of bare TiO_2 [7,8].

The second drawback associated with bare TiO_2 nanoparticles is its weak visible-light photoresponsiveness, thus limiting its opportunity to harness solar light as excitation source. Given the huge potential of solar photocatalysis for practical applications in water treatment [9], it would be desirable to modify bare TiO_2 powders to exhibit enhanced photoresponsiveness under visible-light illumination. Recent studies revealed that TiO_2 could demonstrate increased visible-light photoactivity when the photocatalyst is doped with metal [10,11] and non-metal [12–14] dopants. However, metal dopants have several disadvantages such as thermal instability [11], exorbitant material costs, and possible secondary water contamination (if the metals are toxic). Thus, for realizing the application of semiconductor photocatalysis in water reclamation,

* Corresponding author. Tel.: +65 6790 6933; fax: +65 6791 0676.
E-mail address: cttlim@ntu.edu.sg (T.-T. Lim).

0920-5861/$ – see front matter © 2010 Elsevier B.V. All rights reserved.
doi:10.1016/j.cattod.2010.09.024

the more attractive option is to focus on non-metal dopants. Nitrogen is a promising non-metal dopant as numerous studies have shown that nitrogen-doped TiO_2 manifested pronounced visible-light photoresponsiveness [14,15].

We have undertaken the effort to engineer a bi-functional material, namely nitrogen-doped TiO_2 supported on activated carbon (N-TiO_2/AC) composite. This unique composite potentially offers four-fold benefits for water and wastewater reclamation and reuse, namely (a) minimizes chemical consumption, (b) lowers energy footprint, (c) removes various recalcitrant organic pollutants with diverse characteristics, and (d) produces zero-waste stream. Bisphenol-A (BPA), an endocrine disrupting compound, was chosen as a model pollutant for examination. It is a hydrophobic pollutant with K_{ow} of $10^{3.40}$ [16], Henry's constant of 1×10^{-10} atm-m^3/mol [17], and has high affinity for AC sorption. Furthermore, BPA is found ubiquitously in many water systems, and has been reported to be a potential toxicological threat to living beings [18,19].

For practical applications in water treatment, it is important that the as-synthesized N-TiO_2/AC composites continuously exhibit bi-functionality of adsorption-photocatalysis and also maintain satisfactory durability under prolonged usage. Thus, effective preparation method for this unique composite is crucial to ensure that high removal efficiency of organic pollutants is achieved. This paper aims to discuss the characteristics of N-TiO_2/AC composites prepared by tailored synthesis (sol–gel method incorporating two-stage calcination), and their bi-functional properties for the synergistic removal of hydrophobic organic pollutant in aqueous system. Furthermore, various pertinent aspects such as effect of light wavelength, influence of composite dosage, performance under repeated use and composite photostability are elucidated in this article.

2. Experimental

2.1. Chemicals

Titanium tetraisopropoxide (TTIP) (Merck) was used as titanium precursor. Absolute ethanol was used as solvent. Urea (Merck) was employed the source of nitrogen during wet-chemistry synthesis. HCl (37%) was used for catalyzing sol formation. Hydrogen peroxide (H_2O_2) was obtained from Sigma–Aldrich. BPA was procured from Merck. Degussa P25 was provided by Jebsen & Jessen Chemicals while Hombikat (Sigma–Aldrich) was bought from Sigma–Aldrich. All the abovementioned chemicals were used directly without further purification. Powdered AC (Norit SA UF) was purchased from Behn Meyer, Singapore. The AC was pre-treated in NaOH solution (1.0 M) and subsequently vacuum-dried. All aqueous solutions were prepared using ultrapure water (18.2 MΩ cm).

2.2. Preparation of N-TiO_2/AC composites

The N-TiO_2/AC composites were synthesized via sol–gel method. A solution containing TTIP dissolved in absolute ethanol was firstly prepared. To this solution, absolute ethanol acidified with HCl was added dropwise under vigorous stirring. Subsequently, ultrapure water was added dropwise for hydrolysis and the resulting solution was left to homogenize. Pre-treated AC was then immersed and the solution was left to mix overnight. The slurry suspension was gradually heated to form gel-coated precipitates. After cooling to room temperature, urea solution was added. Finally, the gel-coated precipitates were recovered by centrifugation and vacuum-dried. Additional two rounds of repeated coatings were carried out to achieve more coverage of N-TiO_2 particles on AC surface. Finally, the N-TiO_2/AC powders were calcined in either single-stage (aM) or two-stage (aM-bT), where both a and b denote calcination temperatures, M denotes calcination of 2 h under air atmosphere using muffle furnace, and T denotes calcination of 2 h under NH_3/N_2 atmosphere using tube furnace, respectively. For comparison, N-TiO_2 powders were prepared using same protocol but without addition of AC. Bare TiO_2 powders were prepared without addition of urea and AC, and subsequently calcined under pure N_2 atmosphere in a tube furnace (denoted as T-N_2). Meanwhile, virgin AC calcined at 700 °C under the NH_3/N_2 atmosphere is denoted as AC (700T).

2.3. Characterization of N-TiO_2/AC composites

Crystal structures and mineralogy of N-TiO_2/AC composites were investigated using X-ray diffractometer (Bruker AXS D8 Advance), operating at 40 kV and 40 mA, and with Cu-Kα (λ = 1.54 Å) as the X-ray source. The Brunauer–Emmett–Teller (BET) specific surface areas (S_{BET}) and Barrett–Joyner–Halenda (BJH) pore size distributions were obtained through nitrogen adsorption–desorption isotherm analysis carried out at 77 K (QuantaChrome Autosorb-1 Analyzer). Surface depositions of N-TiO_2 on AC were examined using a scanning electron microscope (SEM) equipped with energy dispersive X-ray spectroscope (EDS) (JSM-6360 microscope with JED-2300 X-ray analyzer). Anchorage of N-TiO_2 on AC and the crystallinity of the supported N-TiO_2 were examined using transmission electron microscope (TEM) (JEOL JEM-2100F microscope). Surface chemistry of N-TiO_2/AC composites was analyzed using X-ray photoelectron spectroscope (XPS) (KratosAXIS Ultra spectrometer) operated with Al-Kα X-ray (1486.71 eV). Binding energies for all elements in XPS were calibrated with reference to adventitious carbon (C 1s = 284.8 eV). Bulk N-TiO_2 (wt.%) in AC was quantified using gravimetry method, i.e. ashing the composite under air atmosphere at 700 °C for 2 h.

2.4. Adsorption experiments

All adsorption studies for BPA were conducted at its natural pH (6.0 ± 0.4). Adsorption kinetics of BPA on AC, AC (700T) and N-TiO_2/AC composites were studied through batch adsorption experiments in the dark, by sampling at selected time intervals. Equilibrium adsorption of BPA was also determined over a range of BPA initial concentrations. Sampled aliquots were filtered through 0.45 μm cellulose acetate membrane syringe filters. Aqueous BPA concentrations were analyzed using high-performance liquid chromatography (HPLC) (Perkin-Elmer). A C18 column (Inertsil ODS-3, 4.6 mm i.d. × 150 mm length, 5 μm) was employed and maintained at 25 °C during analysis. Ultrapure water/acetonitrile (20:80, v/v) was used as the mobile phase at flow rate of 1 mL/min, and 225 nm was set as the BPA detection wavelength for the UV–vis detector.

2.5. Photocatalytic degradation (PCD) experiments

All photocatalytic testings were carried out after adsorption equilibrium in the dark was reached and at the natural pH of BPA. PCD studies were conducted using a solar simulator (Newport, USA) equipped with a 150 W Xe arc lamp. The light intensity of the simulated solar spectrum is ca. one sun power (measured using digital power meter, EDTM). Initial concentration of BPA in the solution was 36 mg/L and the BPA solution volume was 250 mL. Composite dosage of 0.15 g/L, 0.25 g/L and 0.35 g/L were attempted. Dichroic mirrors were used to control light wavelengths in specific ranges of UV irradiation (280–400 nm) and visible-light illumination (420–630 nm). For visible-light (420–630 nm) experiments, an additional polycarbonate filter was used to minimize UV intensity to less than 10 μW/cm^2 (measured using AccuMAX XRP-3000 radiometer). During PCD experiments, aeration by air bubbling was not provided and a quartz cover was provided on top

of the glass photoreactor to minimize evaporation. Aliquots were sampled at pre-determined time intervals. The experiments were carried out in duplicate to provide representative results. For comparison, PCD experiments using comparable photocatalyst loadings were also conducted using unsupported photocatalysts, namely TiO_2, N-TiO_2, P25 and Hombikat (Sigma–Aldrich) as well as binary mixtures of titania with AC. Concentration of total organic species in the bulk solution was analyzed using total organic carbon (TOC) analyzer (Shimadzu, ASI-V). Turbidity of solutions was measured using a turbidimeter (HACH, 2100N). For experiments investigating the performance of repeated usage for N-TiO_2/AC composite, concentrated BPA solution was spiked to the remaining solution to achieve almost the same initial solution volume and adsorption in the dark was carried out to obtain aqueous BPA concentration close to the original equilibrium concentration. Consequently, photocatalytic testings were commenced and the aforementioned procedures were repeated for several runs.

2.6. Photostability experiments

N-TiO_2/AC (400M-700T) composite and virgin AC were added into 250 mL of ultrapure water at the dosage of 0.25 g/L. A 35 W (output power) UVA lamp (Labino), with maximum wavelength (λ_{max}) of 365 nm, was employed as the excitation source. UVA intensity at the top surface of the solution was determined to be ca. 14.5 mW/cm^2 (measured using AccuMAX XRP-3000 radiometer). After irradiation to UVA at pre-determined time intervals, the solution samples were filtered through 0.45 μm membrane syringe filter and the filtrate was analyzed using TOC analyzer. For baseline studies, control experiments were conducted without UVA irradiation.

3. Results and discussion

3.1. Characteristics of N-TiO_2/AC composites

Fig. 1(a) depicts the X-ray diffraction (XRD) pattern for various types of N-TiO_2/AC composites. Crystallite sizes were estimated using the Scherrer's equation [20]. N-TiO_2 nanocrystals growth was found to be enhanced by a factor of ca. 3.3 when the calcination temperature varied from 400 °C to 700 °C (Table 1). By using Spurr and Myers equation [21], the rutile content in N-TiO_2/AC (400M-600T) and N-TiO_2/AC (400M-700T) was estimated to be ca. 15% and 40%, respectively. Thus, photoactive anatase phase was predominant over rutile phase even at high sintering temperature of 700 °C. This suggests that AC might have contributed to the suppression of rutile phase transformation. To confirm this phenomenon, the XRD patterns for both N-TiO_2 (400M-700T) and TiO_2 (400M-700T-N_2) were investigated and the results are shown in Fig. 1(b). It can be seen that bare titania without nitrogen-doping and AC support underwent complete transformation to rutile phase at 700 °C. Nitrogen-doping, on the other hand, slightly abated the phase transformation from anatase to rutile, and this is in agreement with reports published elsewhere [22]. Thus, it is evident that AC played the most significant role in retaining the photoactive anatase phase. It is postulated that the creation of interfacial energy between the surface of AC and N-TiO_2, besides resulted in anti-calcination effect [23], might have also significantly restrained the growth of rutile phase.

From Table 1, it can be seen that increasing calcination temperature led to only slight increment in the bulk N-TiO_2 content (<10%) and minor reduction in the S_{BET} for N-TiO_2/AC composites. This is due to insignificant AC mass loss resulting from high temperature calcination. BJH pore size for all types of N-TiO_2/AC was found to be ca. 3.8 nm, indicating that these composites were mainly mesoporous (data not shown).

Table 1
Physico-chemical characteristics, adsorption capacity and PCD efficiency for selected materials.

Sample	Structural and mineralogy	Surface chemistry	Physical property			Adsorption capacity			PCD efficiency
	Crystallite size[a] (nm)	N[b] (at%)	N-TiO_2[c] (wt.%)	S_{BET}[d] (m^2/g)	V^e (cm^3/g)	S_{max} (mg/g)	K_{ads} (L/mg)	R^2	Initial k_{app}[f] (h^{-1})
P25	25.0	–	–	57.8	0.14	–	–	–	0.20
Hombikat (Sigma–Aldrich)	22.8	–	–	57.9	–	–	–	–	0.19
TiO_2 (400M-700T-N_2)	24.8	–	–	1.15	0.007	–	–	–	0.05
N-TiO_2 (400M-700T)	25.1	0.35	–	2.76	0.014	–	–	–	0.06
N-TiO_2/AC (400M)	7.3	0.63	29%	591	0.31	194 ± 2	0.69 ± 0.09	0.996	0.32
N-TiO_2/AC (400M-500T)	10.6	1.29	31%	556	0.27	229 ± 4	0.73 ± 0.10	0.992	0.47
N-TiO_2/AC (400M-600T)	19.5	1.37	33%	548	0.25	240 ± 3	0.82 ± 0.07	0.991	0.52
N-TiO_2/AC (400M-700T)	24.4	1.43	37%	536	0.25	259 ± 4	1.22 ± 0.22	0.992	0.67
Virgin AC	–	–	–	799	0.39	250 ± 6	1.14 ± 0.03	0.992	–
AC (700T)	–	1.84	–	810	0.35	297 ± 5	6.92 ± 1.44	0.998	–
N-TiO_2 (400M-700T) + AC (700T)	–	–	–	–	–	–	–	–	0.15
P25 + AC	–	–	–	–	–	–	–	–	0.44
Hombikat (Sigma–Aldrich) + AC	–	–	–	–	–	–	–	–	0.42

–, data not available or not determined.
[a] Anatase crystallite size, estimated using Scherrer's equation [20].
[b] Determined via XPS.
[c] Bulk composition of N-TiO_2 in composite, as determined via gravimetry method.
[d] BET specific surface area.
[e] BJH total pore volume.
[f] Data obtained from irradiation under simulated solar spectrum.

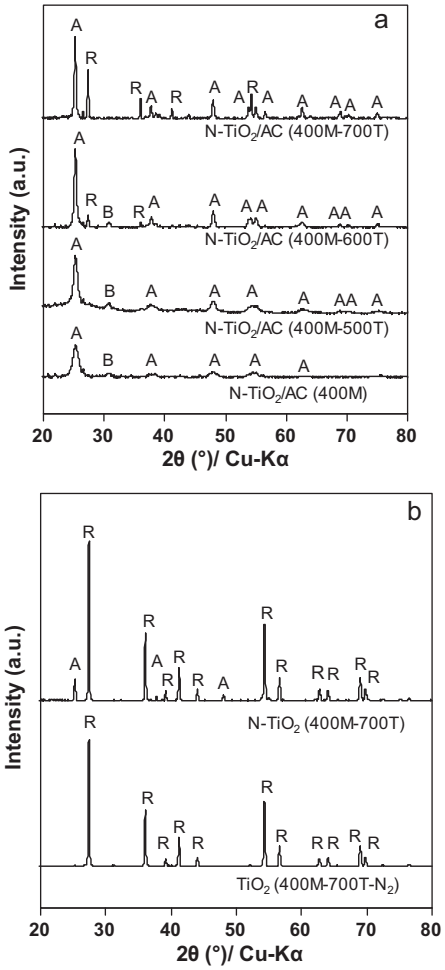

Fig. 1. XRD pattern for (a) various as-synthesized N-TiO_2/AC composites and (b) TiO_2 (400M-700T-N_2) and N-TiO_2 (400M-700T) nanoparticles.

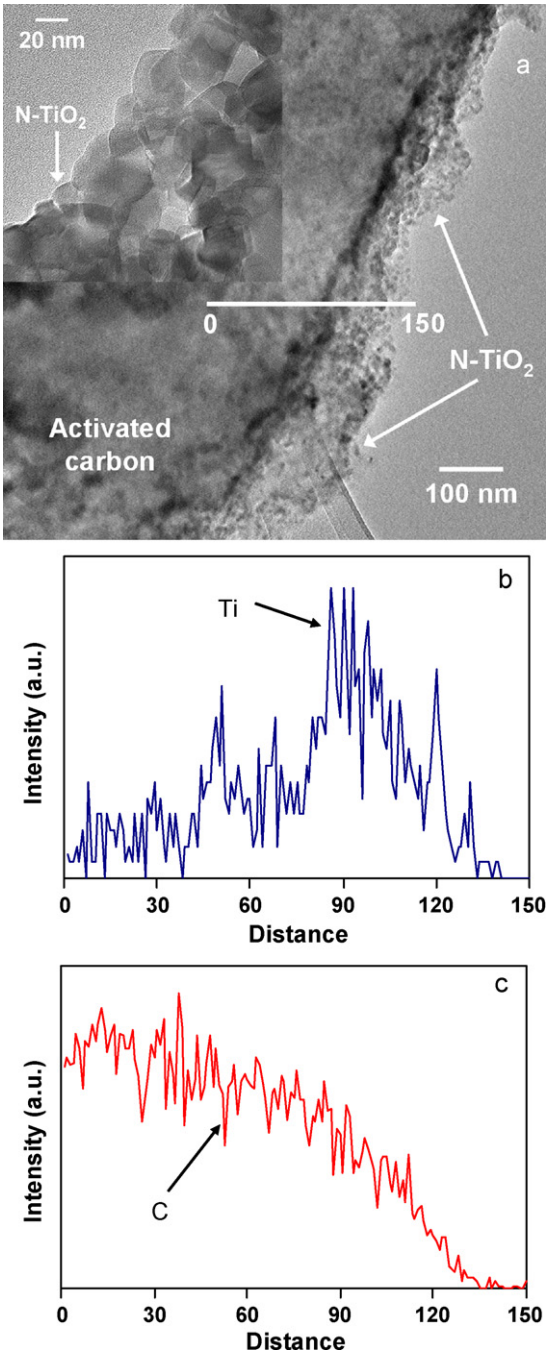

Fig. 2. TEM image for N-TiO_2/AC (400M-700T). (a) Anchorage of N-TiO_2 nanoparticles on the AC surface (inset: the corresponding crystallite sizes of N-TiO_2); (b) Ti intensity–distance profile; (c) C intensity–distance profile.

The amount of nitrogen (Table 1) is largely dependent on the type of calcination condition. It can be observed that with the provision of NH_3/N_2 atmosphere, nitrogen content being doped into the composite was enhanced by at least a factor of 2. The N 1s binding energies for all types of N-TiO_2/AC were found to be located ca. 400 eV (data not shown), indicating that interstitial nitrogen-doping had occurred [14]. To determine the possibility of carbon-doping for the TiO_2, the binding energies of C 1s for TiO_2 (400M-700T-N_2), N-TiO_2 (400M-700T) and all N-TiO_2/AC composites were investigated. The C 1s peak at binding energy of ca. 281.8 eV (indicating substitutional carbon-doping) [24] was not observed in all of the aforementioned samples, indicating undetectable Ti–C bonds.

From the SEM micrograph and the associated elemental mapping obtained for N-TiO_2/AC (400M-700T) (figure not shown), Ti was found to cover a large fraction of the AC surface, indicating well dispersed N-TiO_2 over the AC surface as a result of repeated coating during synthesis. C element was also observed on the elemental map, suggesting that the surface of AC was not entirely covered up by N-TiO_2 nanoparticles, thus preserving carbon adsorption sites on the surface of the composite.

Fig. 2 depicts the anchorage of N-TiO_2 on AC (for N-TiO_2/AC (400M-700T) composite) and the corresponding crystallite size (inset) of N-TiO_2. It can be seen that N-TiO_2 particles adhered onto the surface of AC. The size of N-TiO_2 nanocrystals was observed to be in the ranges of ca. 23–25 nm, and this is in agreement with the estimated average crystallite sizes from Scherrer's equation [20]. To gain insight into the intensity profile of Ti and C elements as a function of distance, EDX analysis was conducted across a selected location on the surface of N-TiO_2/AC composite. The results as shown in Fig. 2(b) reveal that Ti element became more predominant near the interface of N-TiO_2 and AC. The greater amount of Ti at the interface may likely serve as a seed layer for subsequent deposition of N-TiO_2 nanoparticles. Meanwhile, the slight increase of C element for distance ranges 90–150 may be ascribed to some residual AC particles located underneath the N-TiO_2 crystals.

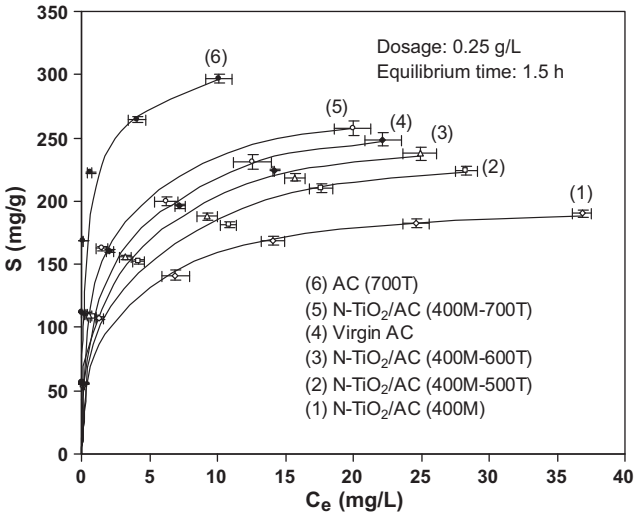

Fig. 3. Adsorption isotherm of BPA on various N-TiO_2/AC composites and AC. (*Note*: error bars denotes standard deviation obtained from triplicate datasets)

3.2. Adsorption characteristics

Adsorption kinetics results reveal that 1.5 h was sufficient for AC, AC (700T) and N-TiO_2/AC composites to reach BPA adsorption equilibrium (data not shown). Adsorption isotherm for AC, AC (700T) and various types of N-TiO_2/AC composites was described using Langmuir isotherm model and the results are presented in Fig. 3. The maximum adsorption capacity (S_{max}) and Langmuir adsorption constant (K_{ads}) are shown in Table 1. Due to the deposition of N-TiO_2 on AC surface, adsorption capacity for N-TiO_2/AC composites was expected to be reduced considerably. Interestingly, for composites calcined under NH_3/N_2 atmosphere, an increasing trend of adsorption capacities for BPA with respect to calcination temperature was observed. The trend in elevated sorption capacity may be ascribed to the surface functionalization of AC, as a result from the interaction with ammonia gas, since nitrogen is an inert gas. Moreover, it can be seen that AC (700T) exhibited a significant increase of BPA adsorption as opposed to virgin AC. This is in agreement with some previous studies [25–28], whereby ACs being treated under ammonia gas were found to possess improved adsorption capacities for several types of organic substances. It was suggested that the nitrogen species had modified the surface chemistry of AC. Thus, XPS analysis was carried out on the AC (700T). The results revealed that N 1s was detected on the surface of AC (700T) (Table 1). This implies that nitrogen atoms were chemically bonded with the surface functional groups of AC. The increased adsorption capacity not only permits greater uptake of pollutants from water, but also positively influence the kinetics and extent of photocatalytic efficiency of the N-TiO_2/AC composites.

3.3. PCD performances

3.3.1. Effect of calcination conditions

Fig. 4(a) shows the effect of N-TiO_2/AC calcination conditions on the PCD performance with respect to BPA removal. The kinetics of BPA photodegradation was delineated using pseudo first-order kinetics model, i.e. $\ln(c/c_o) = -k_{app}t$, where c_o denotes the equilibrium concentration of BPA after adsorption in the dark, c denotes the concentration of BPA in the bulk solution at irradiation time t, k_{app} denotes pseudo first-order rate constant and t denotes the irradiation time. Initial k_{app} (for the initial 3 h of irradiation) was chosen because subsequent experimental data appeared to deviate from the linear plot of $\ln(c/c_o)$ vs t due to diminishing BPA con-

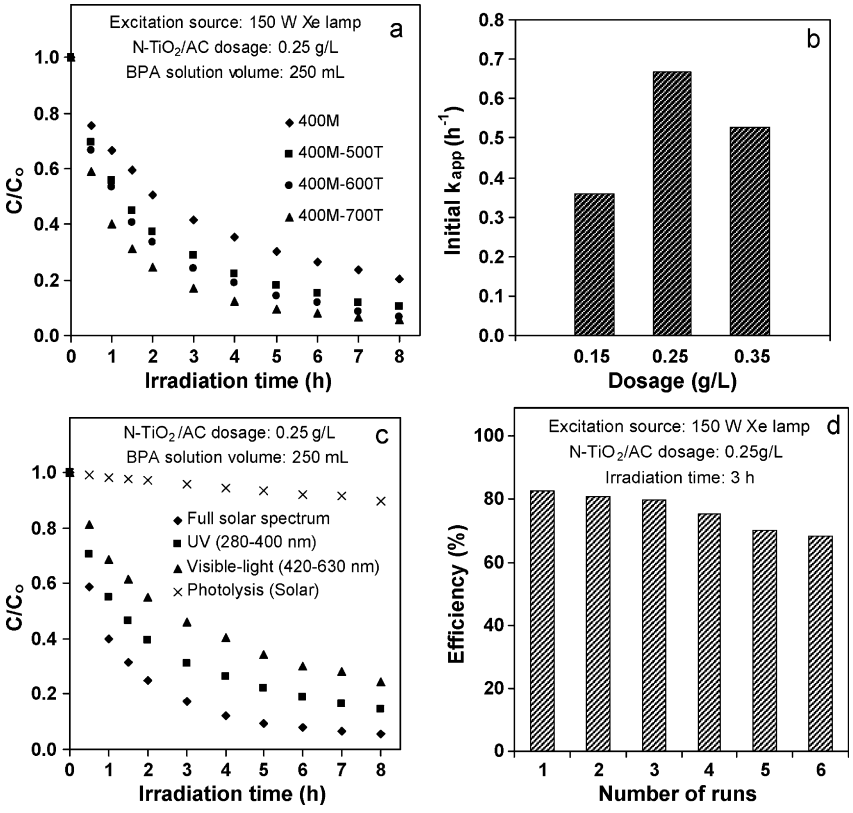

Fig. 4. Influence of photocatalytic degradation. (a) The effect of calcination conditions on the PCD efficiency of various types of N-TiO_2/AC composites, (b) the effect of N-TiO_2/AC (400M-700T) composite dosage on the PCD performance, (c) the effect of light wavelength on governing the photocatalytic activity, as exhibited by N-TiO_2/AC (400M-700T), and (d) performance of repetitive use of N-TiO_2/AC (400M-700T).

centrations in the photoreactor. It was observed that composites which underwent two-stage calcination exhibited enhanced efficiency for BPA photodegradation, with the highest removal (>90%) being exhibited by N-TiO_2/AC (400M-700T) within 8 h of simulated solar irradiation. The remarkable PCD performance of bi-functional N-TiO_2/AC (400M-700T) can be ascribed to the synergistic effect of adsorption-photocatalysis. During adsorption in the dark, AC would concentrate high amounts of BPA to be near the surface of supported N-TiO_2. Upon light irradiation, photocatalysis process would occur and as a result, highly oxidizing species such as holes (h^+) or hydroxyl radicals (•OH) would be produced and these species served to efficiently photodegrade BPA on the surface of N-TiO_2. In addition, the production of highly crystalline nitrogen-doped anatase–rutile mixture for N-TiO_2/AC (400M-700T) is desirable. For anatase–rutile mixture, photogenerated electrons in the conduction band of anatase are transferred to the conduction band of rutile, thus preventing charge carriers recombination and yielding high photocatalytic activity [29,30]. It has been reported that nitrogen doping induced the generation of localized states within the bandgap (slightly above the valence band maximum), and these states could serve as trapping sites for photogenerated holes for efficient photocatalytic reactions [14,31]. Therefore, N-doped anatase–rutile mixture potentially further enhanced photocatalytic activity because the occurrences of charge carriers recombination were effectively minimized. Furthermore, by having the first stage of calcination in air atmosphere, organic residuals from wet-synthesis can be eliminated, thus permitting greater exposure of titania surface to receive the incident light. Thus, N-TiO_2/AC (400M-700T) was used for further investigations.

3.3.2. Effect of composite dosage

The influence of composite dosage on the PCD of BPA is presented in Fig. 4(b). The turbidity level for dosage of 0.25 g/L was larger than of 0.15 g/L by a factor of ca. 1.4, while smaller than that of 0.35 g/L by a factor of ca. 0.80. In the case of 0.15 g/L dosage, although light distribution in the whole photoreactor was least hindered, the amount of N-TiO_2 were unlikely to be adequate for optimum PCD rate. On the other hand, while 0.35 g/L of dosage provided greater amount of N-TiO_2 particles, its high turbidity resulted in greatest light attenuation in the photoreactor. Thus, 0.25 g/L was identified to be the optimum dosage for subsequent PCD examinations.

3.3.3. Effect of light wavelength

The effect of various types of light wavelength on BPA photodegradation as exhibited by N-TiO_2/AC (400M-700T) is as shown in Fig. 4(c). It can be seen that the composite exhibited satisfactory photocatalytic activity for all ranges of light spectrum investigated, i.e. the simulated solar spectrum, UV (280–400 nm) and visible-light (420–630 nm), with initial k_{app} of 0.67 h^{-1}, 0.44 h^{-1}, and 0.29 h^{-1}, respectively. TOC analysis at the end of the experiments revealed that the reduction of total organic species in the bulk solution also followed similar trend, i.e. 72%, 60% and 45% of removal efficiencies for irradiations under the simulated solar light, UV and visible-light, respectively. The effect of photolysis under simulated solar light on the removal of BPA was negligible (ca. 10%). For comparison, a separate study was also carried out to determine the effect of simulated solar light on two different photocatalytic systems, i.e. unsupported photocatalyst system involving TiO_2 (400M-700T-N_2), N-TiO_2 (400M-700T), P25 and also binary mixture systems of titania with AC, namely N-TiO_2 (400M-700T) + AC (700T), P25 + AC and Hombikat (Sigma–Aldrich) + AC. The obtained results are presented in Table 1. It can be observed that under simulated solar light irradiation, N-TiO_2/AC (400M-700T) composite exhibited greater efficiency of BPA photodegradation as compared to systems of unsupported photocatalysts and binary mixtures of titania + AC, indicating the superiority of synergistic adsorption-photocatalysis processes.

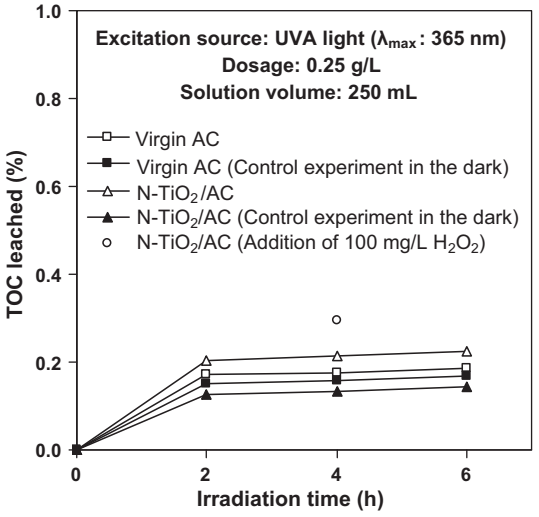

Fig. 5. Time-dependent profile for the amount of leached TOC from samples.

3.3.4. Repeated usage under simulated solar light irradiation

The performance of repetitive usage for N-TiO_2/AC (400M-700T) is presented in Fig. 4(d). It can be observed that the composite exhibited satisfactory PCD performance, whereby ca. 80% of photonic efficiency (as compared to the 1st run) could be maintained after the end of 6th experimental run. This suggests that the composite may have reasonably well mechanical stability, in which the good adherence of N-TiO_2 nanoparticles on AC surface maintained the synergistic effect of adsorption-PCD hybrid processes. The results also indicate the viability of employing solar irradiation as the excitation source to regenerate exhausted N-TiO_2/AC.

3.3.5. Photostability

Fig. 5 shows that amount of TOC being leached from N-TiO_2/AC (400M-700T) and virgin AC in ultrapure water upon irradiation with high intensity UVA. As baseline studies, leaching in the dark were conducted for both samples to determine the amount of inherent organic impurities which are readily released into water. The obtained trend seems to suggest that TOC concentration would approach a steady-state condition. The results show that both N-TiO_2/AC (400M-700T) and virgin AC were photostable after 6 h of UVA irradiation, with the amount of TOC leached to be less than ca. 0.1% and 0.05%, respectively.

In the case of N-TiO_2/AC (400M-700T), although the amount of carbon in contact with UV was reduced due to the deposition of N-TiO_2 nanoparticles, increased production of •OH in the N-TiO_2/AC (400M-700T) composite system apparently resulted in relatively more amount of leached TOC. To investigate the role of •OH in the aqueous system, an additional study was carried out to subject N-TiO_2/AC (400M-700T) under 4 h of UV irradiation, but with addition of 100 mg/L H_2O_2. The results indicated ca. 1.4 increment factor of TOC leaching as compared to the case without H_2O_2 addition, thus confirming the oxidizing effect of •OH radicals. However, since UV intensity in the solar spectrum is lesser than the UV intensity employed in this photostability experiment, it can be inferred that the structural integrity of N-TiO_2/AC composites will be even less affected under irradiation of solar light. Thus, this assures the good durability of the N-TiO_2/AC (400M-700T) composite under prolonged solar irradiation.

4. Conclusion

Various types of dual-functional composites (N-TiO_2/AC) were prepared by sol–gel method with the incorporation of two-stage calcination protocol and these samples were thoroughly characterized. The best performing composite, viz. N-TiO_2/AC (400M-700T), exhibited high adsorption capacity for BPA, showed good photocatalytic activity under all investigated ranges of light wavelength and demonstrated the potential for reuse. N-TiO_2/AC (400M-700T) also demonstrated superior PCD performance as compared to all investigated systems of unsupported photocatalysts (including commercial titania) and binary mixtures of titania + AC. Photostability studies indicated that the N-TiO_2/AC composite was durable. The synergism arising from adsorption-photocatalysis processes of N-TiO_2/AC composite potentially permits the tapping of solar light to continuously remove various hydrophobic organics in water, thus potentially yields significant cost and energy saving, along with the production of zero-waste stream.

Acknowledgements

The research group acknowledges the financial support provided by the National Research Foundation (NRF), Singapore through project EWI RFP 0802-11. Pow-Seng Yap is indebted to Nanyang Technological University (NTU) for the award of a PhD research scholarship.

Appendix A. Supplementary data

Supplementary data associated with this article can be found, in the online version, at doi:10.1016/j.cattod.2010.09.024.

References

[1] M.R. Hoffmann, S.T. Martin, W. Choi, D.W. Bahnemann, Chem. Rev. 95 (1995) 69–96.
[2] B. Zhu, L. Zou, J. Environ. Manage. 90 (2009) 3217–3225.
[3] Q. Wang, D. Yang, D. Chen, Y. Wang, Z. Jiang, J. Nanopart. Res. 9 (2007) 1087–1096.
[4] J. Menesi, L. Korosi, E. Bazso, V. Zollmer, A. Richardt, I. Dekany, Chemosphere 70 (2008) 538–542.
[5] A. Alinsafi, F. Evenou, E.M. Abdulkarim, M.N. Pons, O. Zahraa, A. Benhammou, A. Yaacoubi, A. Nejmeddine, Dyes Pigments 74 (2007) 439–445.
[6] T. Cordero, C. Duchamp, J.-M. Chovelon, C. Ferronato, J. Matos, J. Photochem. Photobiol. A: Chem. 191 (2007) 122–131.
[7] T.T. Lim, P.S. Yap, M. Srinivasan, A.G. Fane, Crit. Rev. Environ. Sci. Technol., Accepted.
[8] G. Li Puma, A. Bono, D. Krishnaiah, J.G. Collin, J. Hazard. Mater. 157 (2008) 209–219.
[9] S. Malato, J. Blanco, A. Vidal, C. Richter, Appl. Catal. B: Environ. 37 (2002) 1–15.
[10] S.W. Lam, K. Chiang, T.M. Lim, R. Amal, G.K.C. Low, Appl. Catal. B: Environ. 72 (2007) 363–372.
[11] W. Choi, A. Termin, M.R. Hoffmann, J. Phys. Chem. 98 (1994) 13669–13679.
[12] A. Zaleska, J.W. Sobczak, E. Grabowska, J. Hupka, Appl. Catal. B: Environ. 78 (2008) 92–100.
[13] T. Ohno, M. Akiyoshi, T. Umebayashi, K. Asai, T. Mitsui, M. Matsumura, Appl. Catal. A: Gen. 265 (2004) 115–121.
[14] C. Di Valentin, E. Finazzi, G. Pacchioni, A. Selloni, S. Livraghi, M.C. Paganini, E. Giamello, Chem. Phys. 339 (2007) 44–56.
[15] R. Asahi, T. Morikawa, T. Ohwaki, K. Aoki, Y. Taga, Science 293 (2001) 269–271.
[16] B. Leverkusen, Grunddatensatz fuer Altsoffe ueber 1000 JATO, Report cited in SIDS (1993) dossier, Dow Europe, 1989.
[17] P.H. Howard, Handbook of Environmental Fate and Exposure Data, Lewis Publishers, Chelsea, MI, 1989.
[18] J.-H. Kang, D. Aasi, Y. Katayama, Crit. Rev. Toxicol. 37 (2007) 607–625.
[19] W.-T. Tsai, J. Environ. Sci. Health Pt. C 24 (2006) 225–255.
[20] P. Debye, P. Scherrer, Phys. Z. 18 (1917) 291–301.
[21] R.A. Spurr, H. Myers, Anal. Chem. 29 (1957) 760–762.
[22] J. Wang, W. Zhu, Y. Zhang, S. Liu, J. Phys. Chem. C 111 (2007) 1010–1014.
[23] Y. Li, S. Zhang, Q. Yu, W. Yin, Appl. Surf. Sci. 253 (2007) 9254–9258.
[24] L. Zhang, R.V. Koka, Mater. Chem. Phys. 57 (1998) 23–32.
[25] J. Przepiórski, J. Hazard. Mater. 135 (2006) 453–456.
[26] W. Cheng, S.A. Dastgheib, T. Karanfil, Water Res. 39 (2005) 2281–2290.
[27] P.A. Quinlivan, L. Li, D.R.U. Knappe, Water Res. 39 (2005) 1663–1673.
[28] E.D. Dimotakis, M.P. Cal, J. Economy, M.J. Rood, S.M. Larson, Environ. Sci. Technol. 29 (1995) 1876–1880.
[29] G. Li, S. Ciston, Z.V. Saponjic, L. Chen, N.M. Dimitrijevic, T. Rajh, K.A. Gray, J. Catal. 253 (2008) 105–110.
[30] T. Kawahara, Y. Konishi, H. Tada, N. Tohge, J. Nishii, S. Ito, Angew. Chem. Int. Ed. 41 (2002) 2811–2813.
[31] R. Beranek, B. Neumann, S. Sakthivel, M. Janczarek, T. Dittrich, H. Tributsch, H. Kisch, Chem. Phys. 339 (2007) 11–19.